J. Fluid Mech. (2006), *vol.* 566, *pp.* 1–9.
doi:10.1017/S0022112006002151 Printed in the United Kingdom

Direct numerical simulation of turbulent flow around a wall-mounted cube: spatio-temporal evolution of large-scale vortices

By ALEXANDER YAKHOT,[1] TOMER ANOR,[1] HEPING LIU[1,2] AND NIKOLAY NIKITIN[3]

[1]The Pearlstone Center for Aeronautical Engineering Studies, Department of Mechanical Engineering, Ben-Gurion University, Beersheva 84105, Israel

[2]Current address: Central Iron & Steel Research Institute, 76 Xueyuan NanLu, Beijing, 100081, China

[3] Institute of Mechanics, Moscow State University, 1 Michurinsky prospect, 119899 Moscow, Russia

(Received 5 April 2006 and in revised form 10 July 2006)

Flow around a wall-mounted cube is an example of a turbulent flow around a three-dimensional bluff body attached to a surface. The main experimentally observed feature of this type of flow is the appearance of complex vortical structures, e.g. a horseshoe vortex originating in front of the body and enveloping it. The current paper is a follow-up to Yakhot, Liu & Nikitin (2006) in which we presented results of direct numerical simulation (DNS) of turbulent flow around a cube. Here, it is shown that unsteadiness of the considered flow is caused by inviscid–viscous interaction between the horseshoe vortex and the narrow band of positive vorticity attached to the surface in front of the cube. Details of the spatio-temporal evolution of large-scale vortical structures, including samples of long-term visualization and turbulence statistics, are presented. For the normal-to-the-wall velocity, in the vicinity of the cube's front face, the results reveal an anomalous probability distribution, namely, a bimodal distribution and one with high kurtosis.

1. Introduction

Turbulent flow in a channel with wall-mounted cubes represents a general engineering configuration that is relevant to many applications. Owing to the simple geometry but complex vortical structures and generic flow phenomena associated with a turbulent flow, this flow has been used for bench-marking purposes to validate turbulence models and numerical methods. The first measurements of the turbulent velocity field, energy balance and heat transfer around a surface-mounted cube were published in the 1990s. Since then, several experiments have been performed on the flow around a single wall-mounted cube in a turbulent channel flow. Results showed that this flow is characterized by the appearance of a horseshoe-type vortex at the windward face, an arc-shaped vortex in the wake of the cube, flow separation at the top and side faces of the cube and vortex shedding. The flow features and experimental data for time-averaged flow quantities have been well documented (Hussein & Martinuzzi 1996; Martinuzzi & Tropea 1993; Meinders, Hanjalić & Martinuzzi 1999; Meinders & Hanjalić 1999). Most numerical studies were performed using the Reynolds-averaged Navier–Stokes (RANS) method with different turbulence models and large-eddy simulations (LES) (Iaccarino *et al.* 2003; Krajnović & Davidson

1999; Rodi *et al.* 1997; Shah & Ferziger 1997). For the flow considered in the present study, however, the RANS approach could not reproduce the details of the complex fluid structure near the wall, e.g. the converging–diverging horseshoe vortex and the separation of the boundary layer in front of the cube, nor the separation length behind the cube. This inability is commonly attributed to the fact that the RANS approach disregards the unsteady interaction of large-scale vortices. On the other hand, global flow features and characteristics predicted by LES and more recently by unsteady RANS-based modelling (Iaccarino *et al.* 2003) showed good agreement with experimental data.

The current paper is a follow-up to Yakhot, Liu & Nikitin (2006) where we presented DNS-based results of turbulence statistics including mean-square intensities, Reynolds shear stresses, turbulence kinetic energy and dissipation rate. In that paper, we drew attention to the negative turbulence production obtained in the region in front of the cube (where the main horseshoe vortex originates). This negative production indicates the non-equilibrium states and the reverse energy transport from small to large scales which are intrinsic features of essentially large-scale anisotropic flows. In the present paper, we report DNS-based results on the spatio-temporal evolution of large-scale vortical structures developing in front of the cube.

2. Results

2.1. *Flow pattern*

In this paper, we use the DNS data of Yakhot *et al.* (2006), where an immersed boundary method was applied for simulating the flow around a wall-mounted cube in a fully developed turbulent channel for a Reynolds number $Re = 5610$, based on the mean velocity (U_m) and the channel height ($3h$). The coordinates and flow parameters presented in this section are non-dimensionalized, and the cube's height, h, and the mean velocity U_m are characteristic length and velocity. The size of the computational domain is $14 \times 3 \times 6.4$ in the streamwise (X), normal to the channel walls (Y) and spanwise (Z) directions, respectively; its inlet and outlet are located at $X = 0$ and $X = 14$, and the cube is located between $3 \leqslant X \leqslant 4$, $0 \leqslant Y \leqslant 1$, $-0.5 \leqslant Z \leqslant 0.5$. The computational grid consists of $181 \times 121 \times 256$ gridpoints in the X-, Y- and Z-directions. A non-uniform mesh was used in the streamwise and wall-normal directions, with gridpoints clustering near the channel and cube walls. The finest grid spacing is of the order $\Delta X_{min} = 0.024$ near the cube's front and rear walls and $\Delta Y_{min} = 0.006$ near the channel and cube's top walls. To generate a DNS-based fully developed turbulent flow to be used as the inlet condition to the channel with a cube, the computational domain also includes an entrance channel measuring $9 \times 3 \times 6.4$. The computational grid in the entrance channel had $64 \times 121 \times 256$ gridpoints in the X-, Y- and Z-directions, respectively. Periodic boundary conditions were imposed in the spanwise Z-direction, and convective velocity conditions were prescribed on the downstream outlet boundary. Using periodic boundary conditions in the spanwise direction raises a question about the reliability of the results for the case of a wall-mounted cube in a channel. This issue is beyond the scope of the present study, but the LES results of Shah & Ferziger (1997) were obtained in a computational domain of $10 \times 2 \times 7$ using periodic boundary conditions in the spanwise direction. The spanwise size (7) was chosen to ensure that the blockage effects are small and the results were found to be in good agreement with the experimental data (Martinuzzi & Tropea 1993). In Yakhot *et al.* (2006), the accuracy of the computations was controlled by comparing computational resolution around the cube with Kolmogorov's length scale and by

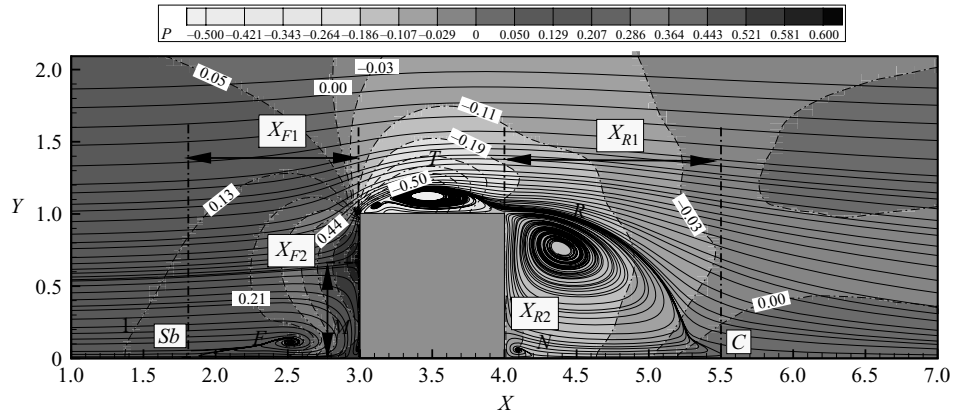

FIGURE 1. Time-averaged streamlines and pressure distribution (background map) on the symmetry plane. Flow is from left to right; for labels, see Yakhot *et al.* (2006).

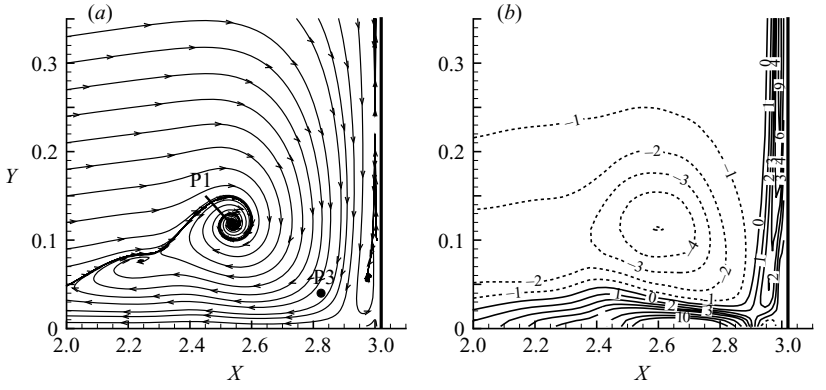

FIGURE 2. (*a*) Time-averaged streamlines. (*b*) Time-averaged spanwise Ω_z-vorticity contours in the symmetry plane $Z = 0$; dashed line: negative vorticity (clockwise rotation), solid line: positive vorticity.

grid refinement. For the grid refinement test, a computational grid of $241 \times 141 \times 256$ gridpoints in the main channel was used while additional gridpoints were added near the front and top of the cube and also near the channel base. The lengths of the main separation regions in front, on the top and behind the cube (see figure 1) obtained on two computational grids were found to be practically identical.

In this paper we decompose the velocity $\boldsymbol{u} = (u_x, u_y, u_z)$ into stationary (time-averaged) and fluctuating parts, $\boldsymbol{u} = \overline{\boldsymbol{U}} + \boldsymbol{u}'$, and use the following notation: $\overline{\boldsymbol{U}} = (\overline{U}, \overline{V}, \overline{W})$, $\boldsymbol{u}' = (u, v, w)$. Figure 1 shows the time-averaged streamlines and pressure distribution (the background) at the symmetry plane. In figure 2(*a*), we show the time-averaged streamlines in front of the cube, the region of primary interest in this paper. Figure 2(*a*) reproduces with noteworthy similarity the pattern experimentally obtained by Martinuzzi & Tropea (1993). The streamlines clearly depict two nodal points (foci). One node at the point (2.55, 0.12) is related to the primary (horseshoe) vortex. The origin of the second node at the point (2.25, 0.07) will be elucidated below. This topology was analysed according to kinematical principles for flows around surface-mounted obstacles by Hunt *et al.* (1978). However, they assumed a saddle point between the nodes, which was not observed in our DNS data. Figure 2(*b*)

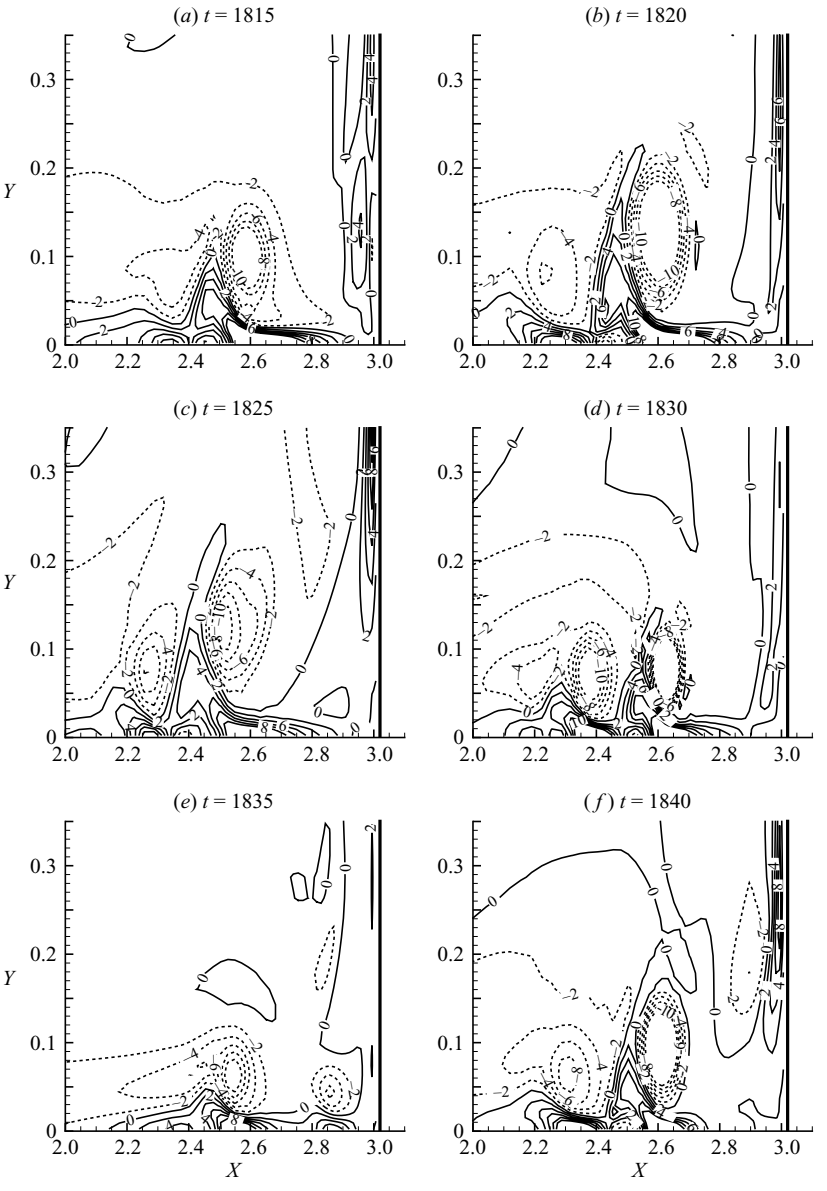

FIGURE 3. Contours of the instantaneous spanwise vorticity ω_z in the symmetry plane $Z = 0$ in front of the cube. Flow is from left to right; the cube's front face is at $X = 3$; dashed line: negative vorticity (clockwise rotation), solid line: positive vorticity.

shows contours of the time-averaged spanwise vorticity $\Omega_z = \partial\overline{V}/\partial x - \partial\overline{U}/\partial y$ in the symmetry plane. From figure 2(*b*), we can see that as a result of the mean backflow, the vorticity changes its sign close to the wall. This change induces an inflection in the mean velocity profile, which usually leads to instability.

2.2. *Large-scale vortices*

DNS data on the evolution of the instantaneous spanwise vorticity $\omega_z = \partial u_y/\partial x - \partial u_x/\partial y$ are shown in figure 3. The dominant characteristic frequency of the vertical

velocity (v) at the point P1(2.53, 0.12, 0) (which is in the vicinity of the horseshoe vortex centre, figure 2a) was found to be about 0.08. This value corresponds to the non-dimensional characteristic time of about 12.5. The dynamics of the horseshoe vortex is imposed by the positive vorticity concentrated into a very narrow band in the streamwise direction. Its interaction with the horseshoe vortex of opposite negative sign leads to ejection of the low-speed fluid away from the wall, as illustrated by the solid lines in figure 3(a). At an earlier stage, on the left of the lifted-up fluid, we can observe the development of a secondary vortex of the same sign as the primary horseshoe vortex. The second nodal point, indicated in figure 2, is a vestige of that secondary vortex. As lifted-up fluid is entrained by the main stream, it wraps around the horseshoe vortex (figure 3b, c) causing it to weaken (figure 3d, e). We speculate that two vortices shown in figure 3(e) are part of the same event illustrated in figures 3(a–d), while figure 3(f) depicts a successive event very similar to that shown figure 3(b). Figure 3 illustrates a scenario of an unsteady inviscid–viscous interaction between the horseshoe vortex and the narrow positive vorticity-loaded band attached to the wall. These events match those discussed in Doligalski, Smith & Walker (1994) and Simpson (2001), that were based upon experimental findings.

Hunt, Wray & Moin (1988) defined an 'eddy' (structure) as a region with a positive second invariant $Q = 0.5(\|\boldsymbol{\Omega}\|^2 - \|\boldsymbol{S}\|^2)$, where $\|\boldsymbol{S}\| = [\mathrm{Tr}\,(\boldsymbol{S}\boldsymbol{S}^t)]^{1/2}$, $\|\boldsymbol{\Omega}\| = [\mathrm{Tr}\,(\boldsymbol{\Omega}\boldsymbol{\Omega}^t)]^{1/2}$ and $\boldsymbol{S}$ and $\boldsymbol{\Omega}$ are the symmetric and antisymmetric components of the velocity gradient tensor $\nabla\boldsymbol{u} \equiv \partial u_i/\partial x_j$, i.e. $S_{ij} = 0.5(\partial u_i/\partial x_j + \partial u_j/\partial x_i)$ and $\Omega_{ij} = 0.5(\partial u_i/\partial x_j - \partial u_j/\partial x_i)$. Positive Q indicates that the vorticity prevails over shear. By definition, Q is the source term in the Poisson equation for pressure $\nabla^2 p = 2Q$, and the criterion $Q > 0$ indicates the low-pressure regions that can be associated with vortical structures. In figure 4, we present the iso-surfaces of $Q = 10$ at the same time instants as the instantaneous vorticity contours in figure 3. The surfaces in figure 4(c–e) also indicate a weakening of the vortical structure. Sometimes, the vortex structure in front of the cube collapses, as shown in figure 5, though this is a very rare event. Comparing figures 4 and 3 suggests that two-dimensional vorticity contours are the vestiges of the Q-iso-surfaces on the symmetry plane $Z = 0$. However, the ability of the Q-criterion to detect the location and size of a vortical structure is not quite so obvious (Jeong & Hussain 1995).

In the following, we present the results related to the fluctuating velocity field $\boldsymbol{u}' = (u, v, w)$. Figure 6 shows several snapshots of the DNS-based visualization. The alternation of the positive and negative velocity strips ('streaks') indicates coherent vortical structures. Figures 3 and 6 show patterns obtained at the same time instants. In figure 6, we can recognize the dark strips (ejection) and imprints of the rotating clockwise primary and secondary vortices, namely the light strips of the negative v. The elongated patterns of the fluctuating vertical velocity point out a reciprocating motion of the vortical structures in the near-wall region.

2.3. *Turbulence statistics*

DNS-based visualization has revealed qualitatively the chaotic motion of the vortical structures in front of the cube. To obtain turbulence statistics and quantitative measurements of this phenomenon, data were collected at points selected near the wall during the time for period of 1700 time units for intervals of $\Delta t = 0.005$. We computed the velocity probability distribution function (PDF), skewness (S) and kurtosis (Ku).

In figure 7(a), the PDF curve suggests a 'bimodal' distribution for the fluctuating vertical v-velocity as was also experimentally obtained by Hussein & Martinuzzi (1996). This bimodality may indicate that the sample is not homogenous and that

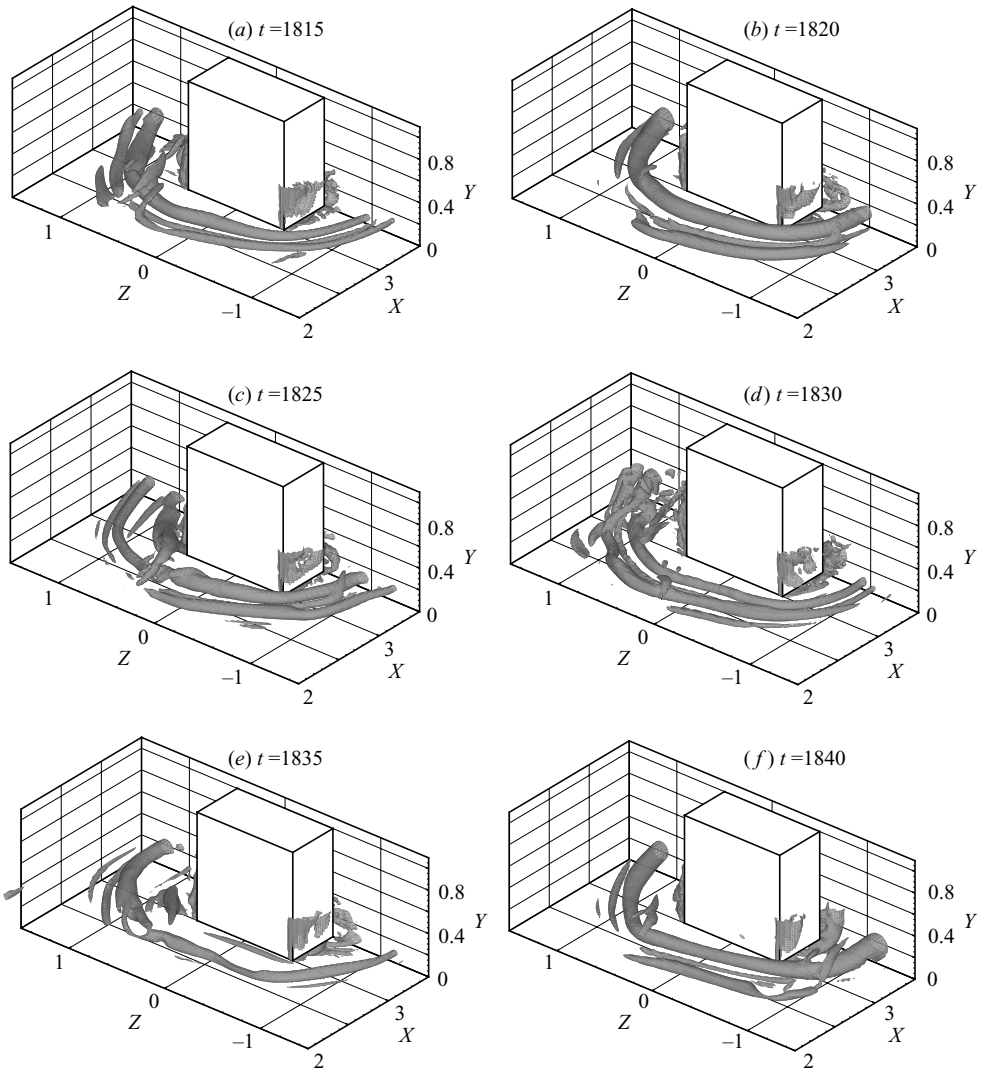

FIGURE 4. Instantaneous iso-surfaces of $Q = 10$.

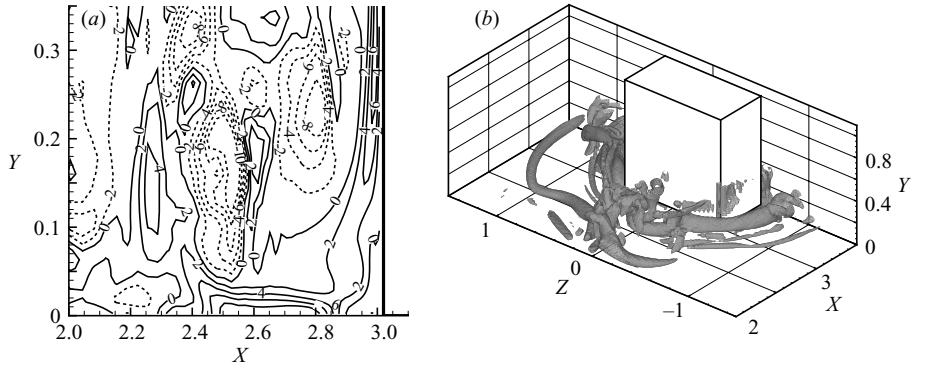

FIGURE 5. (*a*) Instantaneous spanwise ω_z-vorticity contours in the symmetry plane and (*b*) iso-surfaces of $Q = 10$ at $t = 1680$.

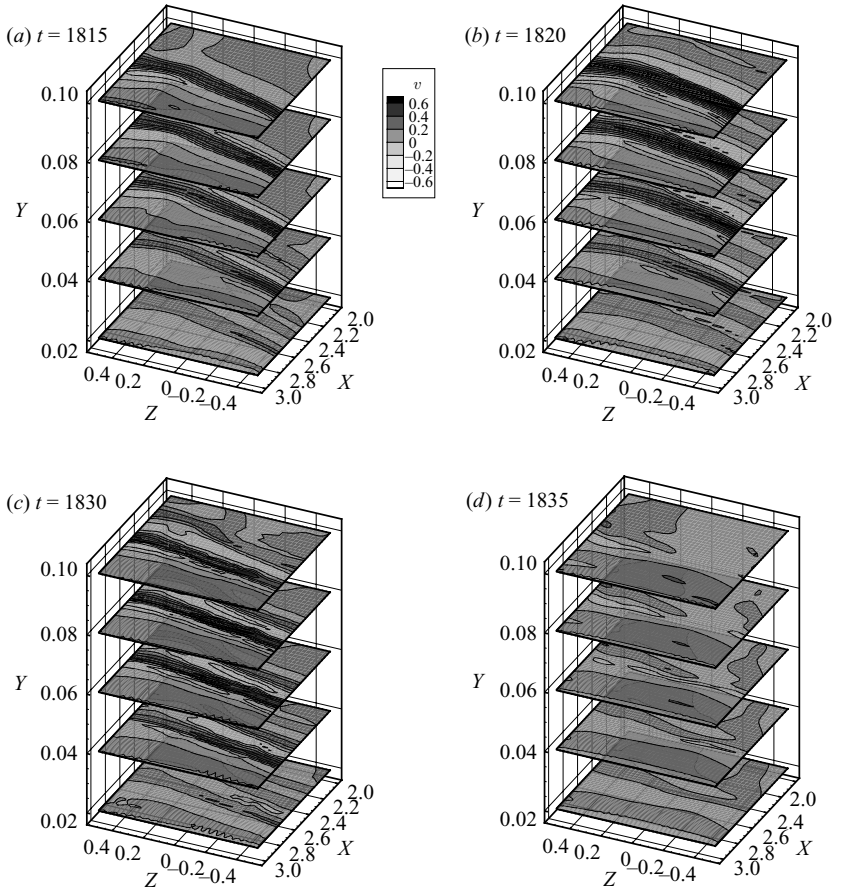

FIGURE 6. Instantaneous fluctuating v-velocity field map in front of the cube on different Y-planes; the front cube's face is at $X = 3$ (not shown); flow is towards the viewer.

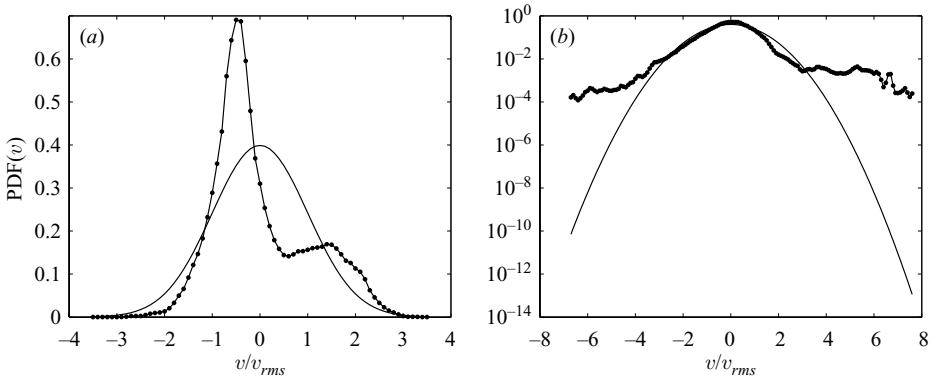

FIGURE 7. PDF(v) vs. v/v_{rms} in front of the cube. The PDF is centred around a time-averaged value and normalized by v_{rms}; solid: Gaussian distribution. (*a*) Point P1(2.53, 0.12, 0), $\overline{V} = 0.013$, $v_{rms} = 0.33$, $Ku = 2.8$, $S = 0.7$; (*b*) point P3(2.82, 0.04, 0.0), $\overline{V} = -0.12$, $v_{rms} = 0.07$, $Ku = 10.4$, $S = 0.86$.

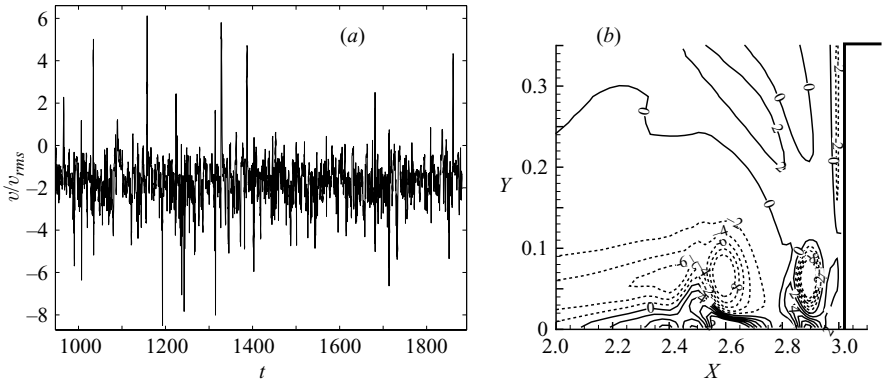

FIGURE 8. (a) Point P3(2.82, 0.04, 0.0), time trace of v-velocity component normalized by its root-mean-square (rms) value; the dominant characteristic frequency $f = 0.105$. (b) Instantaneous spanwise ω_z-vorticity contours in the symmetry plane, $t = 1860$.

observations may arise from two 'overlapping' distributions. In our case, this phenomenon can mainly be attributed to the interaction of the ejected fluid with the primary and secondary vortices, and implies that when a flow aperiodically switches from one mode to another, high-momentum fluid sweeps toward the wall, or low-momentum fluid is ejected away from the wall. At the sampling point P1(2.53, 0.12, 0), the time-averaged vertical velocity is small positive, $\overline{V} = 0.013$. The clearly pronounced peak at $v/v_{rms} \equiv (u_y - \overline{V})/v_{rms} \approx -0.5$ corresponds to the instantaneous vertical velocity $u_y \approx -0.15$, which means that the fluid is sweeping towards the wall (e.g. see figure 3d). The second peak in figure 7(a) depicts an ejection mode where the primary vortex entrains the near-wall fluid (figure 3c). The fact that we did not obtain the camelback shape usually associated with a bimodal distribution may result from the choice of a sampling point where the time-averaged vertical velocity turned out to be small.

In Yakhot *et al.* (2006), we reported that maximum negative turbulence energy production at the symmetry plane $Z = 0$ was obtained in the vicinity of the point P3(2.82, 0.04, 0.0) marked in figure 2(a). The probability distribution of the u and w velocity components at that point was found to be Gaussian. In contrast, figure 7(b) shows a non-Gaussian probability distribution of the vertical velocity v with kurtosis $Ku = 10.4$ instead of a Gaussian value of 3. This anomalously high kurtosis indicates the spatio-temporal intermittent nature of turbulence in that region. The time trace in figure 8(a) shows infrequent spikes with very large fluctuations of the vertical velocity, $-8 < v/v_{rms} < 6$. The sequence of positive/negative spikes leads to the deviation from a Gaussian distribution. These spikes may be a result of the ejection/sweeping events being quite rare in this corner region, and implies that the corner space becomes positive-vorticity-loaded with the possibility that a vortex may be generated there. The spanwise vorticity snapshot taken at $t = 1860$ (figure 8b) corresponds to a positive spike that can be seen in figure 8(a) at $t = 1860$ and shows that a vortex has been generated in the vicinity of the sampling point P3(2.82, 0.04, 0.0).

3. Summary

We performed DNS of a flow around a wall-mounted cube in a fully developed turbulent channel and analysed the DNS data on the spatio-temporal evolution of

large-scale vortical structures developing in front of the cube. The results support the view that unsteadiness of this flow caused by inviscid–viscous interaction between the horseshoe vortex and the narrow band of positive vorticity attached to the channel wall in front of the cube. This interaction leads to ejection of the low-momentum fluid away from the wall. The lifted-up fluid is partially swept back by the secondary vortical structure, while the rest is entrained by the main stream, enhancing disturbances there. For selected locations in front of the cube, we present turbulence statistics, including the probability distribution function, skewness and kurtosis. For the vertical velocity component, the results revealed an anomalous probability distribution, namely a bimodal distribution and one with high kurtosis. Both these phenomena stem from the spatio-temporal intermittent nature of turbulence in that region.

This work was supported by the Israel Science Foundation Grant 159/02. The fourth author (N. N.) was also partially supported by the Russian Foundation for Basic Research under Grant 05-01-00607. The first author (A. Y.) is particularly indebted to Professors Victor Yakhot and Fazle Hussain for valuable discussions. Our special gratitude goes to the IUCC, the Inter-University Computation Center, Tel Aviv, where the numerical simulations were carried out on the Cray J90 supercomputer.

REFERENCES

Doligalski, T. L., Smith, C. R. & Walker, J. D. P. 1994 Vortex interaction with walls. *Annu. Rev. Fluid Mech.* **26**, 573–616.

Hunt, J. C. R., Abbel, C. J., Peterka, J. A. & Woo, H. 1978 Kinematic studies of the flows around free or surface-mounted obstacles; applying topology to flow visualization. *J. Fluid Mech.* **86**, 179–200.

Hunt, J. C. R., Wray, A. A. & Moin, P. 1988 Eddies, stream, and convergence zones in turbulent flows. *Center for Turbulence Research Report CTR-S88,* p. 193. Stanford University.

Hussein, H. J. & Martinuzzi, R. J. 1996 Energy balance for turbulent flow around a surface mounted cube placed in a channel. *Phys. Fluids* **8**, 764–780.

Iaccarino, G., Ooi, A., Durbin, P. A. & Behnia, M. 2003 Reynolds averaged simulation of unsteady separated flow. *Intl J. Heat Fluid Flow* **24**, 147–156.

Jeong, J. & Hussain, F. 1995 On the identification of a vortex. *J. Fluid Mech.* **285**, 69–94.

Krajnović, S. & Davidson, L. 1999 Large-eddy simulation of the flow around a surface-mounted cube using a dynamic one-equation subgrid model. *First Intl Symp. on Turbulence and Shear Flow Phenomena.* (ed. S. Banerjee & J. Eaton), Begel House, Inc., New York.

Martinuzzi, R. & Tropea, C. 1993 The flow around surface-mounted, prismatic obstacles placed in a fully developed channel flow. *Trans. ASME: J. Fluids Engng* **115**, 85–91.

Meinders, E. R. & Hanjalić, K. 1999 Vortex structure and heat transfer in turbulent flow over a wall-mounted matrix of cubes. *Intl J. Heat Fluid Flow* **20**, 255–267.

Meinders, E. R., Hanjalić, K. & Martinuzzi, R. J. 1999 Experimental study of the local convection heat transfer from a wall-mounted cube in turbulent channel flow. *Trans. ASME: J. Heat Transfer* **121**, 564–573.

Rodi, W., Ferziger, J., Breuer, M. & Pourquié, M. 1997 Status of large-eddy simulation: results of a workshop. *Trans. ASME: J. Fluids Engng* **119**, 248–262.

Shah, K. B. & Ferziger, J. H. 1997 A fluid mechanicians view of wind engineering: large eddy simulation of flow past a cubic obstacle. *J. Wind Engng Ind. Aero.* **67/68**, 211–224.

Simpson, R. L. 2001 Junction flows. *Annu. Rev. Fluid Mech.* **33**, 415–443.

Yakhot, A., Liu, H. P. & Nikitin, N. 2006 Turbulent flow around a wall-mounted cube: a direct numerical simulation. *Intl J. Heat Fluid Flow* (to appear), available online DOI:10.1016/j.ijheatfluidflow.2006.02.026.